Theoretical aspects of solid hydrogen halides under pressure

Robert W. Jansen, Rita Bertoncini,* and David A. Pinnick
Department of Physics, Arizona State University, Tempe, Arizona 85287

Allen I. Katz
Los Alamos National Laboratory, The University of California, Los Alamos, New Mexico 87545
and Department of Physics, Arizona State University, Tempe, Arizona 85287

R. C. Hanson and Otto F. Sankey
Department of Physics, Arizona State University, Tempe, Arizona 85287

Michael O'Keeffe
Department of Chemistry, Arizona State University, Tempe, Arizona 85287
(Received 24 November 1986)

The electronic and dynamic properties of the solid phases of HF, HCl, and HBr under pressure are studied theoretically. A simple model is constructed so that the pressure-dependent properties of these systems and possibly other hydrogen-bonded systems can be studied in terms of a few parameters. The model predicts quite simply the pressure dependence of the stretching-mode frequency and the nature of the phase transition from the molecular hydrogen-bonded phase to a new symmetrical hydrogen-bonded (nonmolecular) phase. Quantum effects due to the light hydrogen atom are taken into account within a many-body Hartree approximation. New experimental data on the pressure dependence of the symmetric-stretching-mode frequency in HF is presented. The possibility of soliton formation is discussed and it is shown how pressure may act as a unique tuner to adjust the energetics of these nonlinear excitations. In addition, we report the results of our *ab initio* calculations of the total energy of ringlike structures of HF and the first *ab initio* pseudopotential calculation of the band structure and total energy of solid HBr. The calculations for HF are within the Hartree-Fock approximation, while those of solid HBr are within the local-density approximation and have been simplified by considering a linear instead of a zigzag geometry. The use of the local-density approximation for hydrogen is also discussed.

I. INTRODUCTION

Hydrogen bonding is one of the five fundamental bonding mechanisms in solids. Although the line distinguishing one form of bonding from another is in some cases ambiguous (e.g., II-VI compounds being partly covalent and partly ionic), it is generally not so for the hydrogen bond since it gives rise to unusual and diverse structures. For example, the prototype hydrogen-bonded solid, H_2O ice, forms a complicated three-dimensional solid structure with many phases occurring under pressure.

Much of the recent interest in hydrogen-bonded solids under pressure has been generated because of the expected transition to other bonding mechanisms. In H_2O, a transition is expected from a molecular hydrogen-bonded phase to a phase X with symmetrical hydrogen bonds. Theoretical studies[1] of the transition to this symmetric phase predict a strongly first-order transition. Recent Raman- (Ref. 2) and Brillouin- (Ref. 3) scattering studies give evidence for this phase X of ice at 42 GPa. This work on ice has prompted us to study even simpler hydrogen-bonded solids. In the present study we focus on the simplest, predominantly one-dimensional, hydrogen-bonded solids which are the hydrogen halides HF, HCl, and HBr.

Low-temperature solid hydrogen halides HF, HCl, and HBr have been studied experimentally for many years. X-ray data[4] and neutron diffraction studies[5] have revealed that these compounds form a molecular base-centered-orthorhombic crystal with hydrogen halide molecular pairs arranged in parallel "kinked" chains along one direction of the crystal. NMR studies[6] have also been used to obtain information on the position of the hydrogen atoms within these chains. Spring constants extracted from vibrational frequencies associated with the hydrogen atom have also been obtained using Raman scattering[7–10] and infrared absorption.[7,11,12] The anisotropy of the elastic and photoelastic properties of HF have recently been studied under pressure by Brillouin scattering by Lee *et al.*[13] up to ~ 120 kbar. Studies have been reported by Hanson and co-workers[9,14] and Holzapfel and co-workers[10] on the Raman modes in HCl and HBr under pressure. Johannsen *et al.*[10] show evidence for the transition to the symmetric phase of HBr. The related hydrogen-halide HI forms a different, more complicated geometry,[15] and will not be dealt with specifically here.

We will show that the light mass of the hydrogen atom and the nature of the hydrogen bond are expected to give the hydrogen-halide crystals many peculiar and interesting properties. These crystals are ideal to study because

they form very simple hydrogen bonded structures. At low pressure, solid hydrogen-halide crystals form molecular chains in which the hydrogen atom is covalently bonded to one or the other of the adjacent halide atoms in the chain. Under pressure, we expect this molecular structure to change and the system to be driven to a symmetric phase where the hydrogen is bonded equally to both of its nearest-neighboring halide atoms in the chain. Before this phase transition occurs, it is expected that the light mass of hydrogen will allow quantum tunneling of the hydrogen from one halide to the adjacent halide.

To understand the nature of these systems a number of sophisticated theoretical computations have been carried out. Most of these calculations have focused on HF (Refs. 16—23) and have used mainly various Hartree-Fock all electron methods. In many cases these calculations have used one-dimensional linear-chain models. These studies have predicted equilibrium geometries, electronic band structures, and force constants of HF for both straight- and kinked-chain models. The halide F was used in these calculations because HF has only eight electrons per molecule and is therefore of manageable size in a Hartree-Fock or other all-electron, *ab initio* calculation.

In this paper we begin a theoretical investigation of the properties of solid hydrogen halides under pressure. Our major interest is the nature of the phase transition from the molecular hydrogen-bonded phase to a new symmetric hydrogen-bonded phase. Our approach is to blend simple models with the results of state-of-the-art *ab initio* calculations. In Sec. II we describe a simple model to understand qualitatively and physically the behavior of solid hydrogen halides under pressure. The construction of a simple model allows us to incorporate in an approximate manner, the quantum and many-body effects associated with the phase transition. The simple model also predicts the formation of solitons in these systems and demonstrates how pressure can be used as a "tuning knob" for their properties. In Sec. III we describe our *ab initio* pseudopotential calculations for a three-dimensional crystal of linear HBr chains. To our knowledge these are the first such calculations of solid HBr. We have computed the band structure and total energy of the crystal as a function of the chain lattice parameter and hydrogen position. The calculations were performed using the local-density approximation and a pseudopotential is used for the Br valence electrons. In Sec. IV we describe the results of our *ab initio* total energy Hartree-Fock calculation of the phase transition to the symmetric phase using a H_6F_6 ring. Finally, in Sec. V we give our conclusions.

II. MODEL CALCULATIONS

We first develop a simple model for the pressure dependence of the hydrogen bond in these crystals. Such a model can serve as a basis for a physical understanding of (i) the general behavior of these systems, (ii) the nonlinearities, and (iii) the quantum effects due to the light hydrogen atom. We also use this model to parametrize the results of our *ab initio* calculations discussed in Secs. III and IV.

At low temperatures these compounds form base-centered-orthorhombic crystals consisting of parallel polarized zigzag chains of hydrogen bonded molecules with two HX (X=F, Cl, or Br) molecules per unit cell (see Fig. 1). The interchain atoms are held together by weak van der Waals and dipolar forces. Since the major bonding effects are between the hydrogen halide molecules along the chain, we consider, as a model system, a single infinite chain of hydrogen-halide molecules. Due to the relatively heavy mass of the halogen atom, the lattice of the X atoms is considered static, and we focus on the hydrogen motion between two neighboring X's in only one dimension.

A unique feature of such a system is that it has a doubly degenerate ground state. The hydrogen atom (at zero pressure) bonds covalently to just one halide atom forming a HX molecule. These molecular units then bind together forming chains because of the hydrogen bond. The double degeneracy occurs because the stronger covalent bond can be made with either the "left" or "right" halide atom. We refer to these two ground states as the left and the right ground state, and they are shown in Fig. 2. In the left ground state the hydrogen is covalently bonded to the neighboring halide on its left, while it is bonded to the halide on its right in the right ground state.

We now imagine moving all the hydrogen atoms in *unison*. The potential function must have two distinct minima (to reflect the degeneracy), separated by a barrier. To fourth order in the proton position x, this potential function can be analytically expressed by the simple double-well, single-particle "bond" potential for the proton,

$$V(x)=\Phi_B(x^2-b^2)^2/b^4 , \tag{1}$$

where x is the proton position measured from the midpoint between its two neighboring halide atoms. Here Φ_B is the barrier separating the left and right ground states, and equivalent minima occur at the two asymmetric displacements, $x=\pm b$. This potential is sketched in Fig. 3. The potential of Eq. (1) is of course nonlinear (anharmonic) as it must be to produce a degenerate ground state. Allowing each hydrogen atom to move individually (not necessarily in unison) introduces a hydrogen-hydrogen pair potential. To avoid the geometric complexities introduced by the kinks in the zigzag chains, we imagine

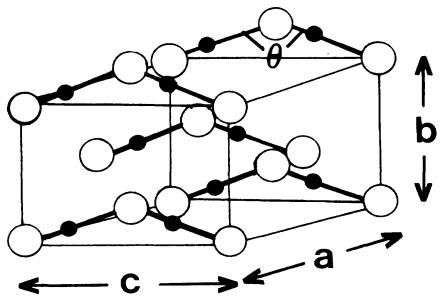

FIG. 1. Crystal structure of HF, HCl, and HBr in their low-temperature base-centered-orthorhombic asymmetric hydrogen phase. The HX molecules are arranged in parallel zigzag chains.

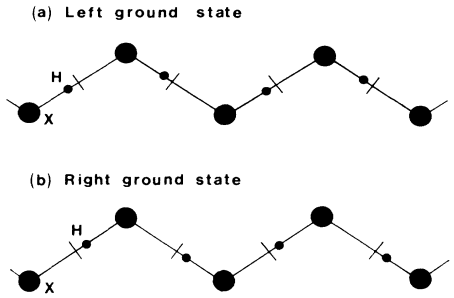

FIG. 2. Diagram showing the two equivalent ground-state positions for hydrogen. In the left (right) ground state, all hydrogen atoms bond covalently with the halide X on their left (right).

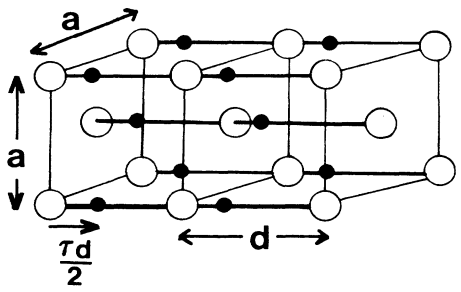

FIG. 4. Simplified base-centered-tetragonal geometry of the hydrogen halide used. The distance between two halide atoms along a chain is d.

stretching the chains so that they are straight and linear (see Fig. 4). Since the major bonding is between H—X and not H—H or X—X, this approximation is not expected to be severe. This reduces the unit cell from four atoms to just two: one hydrogen and one X atom. We take the H-H potential to be a harmonic nearest-neighbor potential with coupling constant K. Thus, the interaction between the hydrogen atom in cell l and those in cells $l\pm1$ is

$$U(x_l,x_{l\pm1})=\tfrac{1}{2}K(x_{l\pm1}-x_l)^2 . \quad (2)$$

Combining Eq. (1) with Eq. (2) we obtain the total many-particle potential function

$$V_{\rm tot}(x)=\sum_l [V(x_l)+U(x_l,x_{l+1})+U(x_l,x_{l-1})] . \quad (3)$$

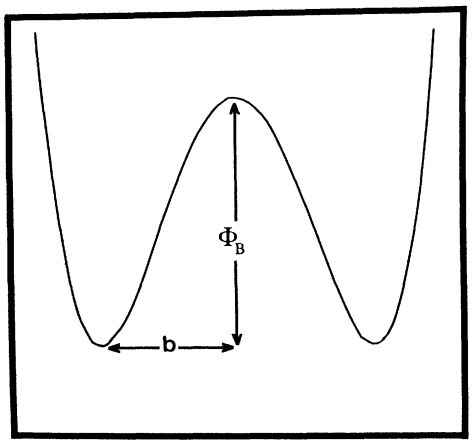

FIG. 3. Sketch of the double-well potential of Eq. (1). The two minima correspond to the left and right ground states where hydrogen is displaced to $\pm b$ from the midpoint between two halides. The barrier separating the two minima is Φ_B.

A. Pressure dependence

As pressure increases, the halide-halide distance decreases and, at some critical pressure P^*, the hydrogen equilibrium position is expected to be located at the midpoint between two halide atoms. This implies that the curvature of $V(x)$ near $x=0$ has changed from being concave downward for $P<P^*$ (two equivalent minima separated by a barrier), to being concave upward for $P>P^*$. At the critical pressure P^*, the potential $V(x)$ is neither concave downward or upward. Let us regard the hydrogen-halide potential function $V(x)$ of Eq. (1) in the more general form of a fourth-order polynomial in x,

$$V(x)=C-Ax^2+Dx^4 . \quad (4)$$

We expect the fourth-order coefficient D to increase as the pressure increases reflecting the stiffening of the lattice, but this increase is not expected to be important in describing the qualitative behavior of the system. The pressure dependence of coefficient C is unimportant in our present discussion since it simply shifts the zero of energy.

Of prime importance is the coefficient A of the quadratic term. This term determines whether the potential is concave upward or downward. Hence, A changes sign as a function of pressure as P passes through P^*. In the spirit of a Landau-type theory, we simply take a linear dependence on pressure of this parameter,

$$A(P)\simeq A(0)(1-P/P^*) . \quad (5)$$

Comparing the coefficients of equal powers of the fourth-order expansion in Eq. (4) with the model analytic expression of Eq. (1) and assuming only the pressure dependence given by Eq. (5), we immediately obtain the pressure dependence of the physically relevant barrier height Φ_B and asymmetric displacement b. The barrier height Φ_B is found to be strongly influenced by pressure and rapidly goes to zero as the pressure approaches the critical value P^*,

$$\Phi_B(P)=\Phi_B(0)(1-P/P^*)^2 . \quad (6)$$

The asymmetric displacement, which is a measure of the position of the hydrogen atom between the two halides, is not as severely dependent on pressure, going to zero at the

phase transition as

$$b(P)=b(0)[(1-P/P^*)]^{1/2} . \quad (7)$$

When b is zero, the hydrogen atom is located at the midpoint between two halides. This simple model predicts a critical exponent of $\frac{1}{2}$ at the phase transition for the order parameter b. The bonding has changed from a hydrogen-bonded molecular solid, to a new symmetric hydrogen bonded form where the molecular identity is lost.

The hydrogen-hydrogen coupling constant K is expected to increase with pressure, so we approximate it as

$$K(P)=K(0)(1+gP/P^*) , \quad (8)$$

where g is a constant. The exact value of g is not important for our purposes here, since the qualitative and most of the quantitative physics of the phase transition is insensitive to reasonable variations of its value. Data on the mode frequencies of HBr indicate a value of g near $\frac{1}{2}$,and we have adopted this value for all materials. Once the functional dependence on pressure of the various parameters appearing in the potential have been established, we proceed to evaluate the single-particle total energy and optic-mode vibrational frequencies.

B. Harmonic approximation

We now consider the dynamics of the hydrogen atoms in the harmonic approximation. This limit is appropriate for small displacements from equilibrium and at low pressures where the barrier is large so that little tunneling occurs. We expand the hydrogen-halide potential, given by Eq. (1), about either of the classical equilibrium position $x=\pm b(P)+\delta$ which gives

$$V(\delta,P)=\tfrac{1}{2}k(P)\delta^2 . \quad (9)$$

The pressure-dependent spring constant $k(P)$ is given by

$$k(P)=8\Phi_B(P)/b^2(P)=k(0)(1-P/P^*) , \quad (10)$$

where the pressure dependence follows from Eqs. (6) and (7). The total harmonic potential energy is then

$$V_{\rm tot}(\delta_1,\delta_2,\ldots)=\tfrac{1}{2}k(P)\sum_l \delta_l^2+\tfrac{1}{2}K(P)\sum_l(\delta_{l+1}-\delta_l)^2 . \quad (11)$$

The eigenmodes of this Hamiltonian can be solved quantum mechanically by a Bogoliubov transformation[24] or classically and leads to the dispersion relation

$$\omega(q)=\{\Omega_0^2+\Omega_1^2[1-\cos(qd)]/2\}^{1/2} , \quad (12)$$

where d is the distance between two neighboring halide atoms (see Fig. 4), and q is the wave vector. The frequencies Ω_0 and Ω_1 are $\Omega_0=\sqrt{k(P)/M}$ and $\Omega_1=\sqrt{4K(P)/M}$, where M is the H-X reduced mass.

At zone center ($q=0$) this mode is the symmetric stretching mode (A_1), $\omega_s=\Omega_0$, where all hydrogen atoms move in phase. Since each H atom moves in unison, only the hydrogen halide potential V affects this motion. This optic-mode frequency has been measured under pressure experimentally by Hanson and co-workers[9] and Johannsen *et al.*[10] These measurements are essentially a probe of the barrier height and asymmetric displacement in the particular combination $(\Phi_B/b^2)^{1/2}$ as in Eq. (10). The pressure dependence of this mode from Eqs. (10) and (12) is

$$\omega_s(P)=\omega_s(0)[(1-P/P^*)]^{1/2} . \quad (13)$$

Note that the frequency is predicted to go down with increasing pressure, and is a soft mode going to zero at the phase transition pressure P^*. This is unlike molecular solids such as N_2 in which the "vibron" frequency increases with pressure.[25] The limit of zero frequency is an artifact of the harmonic approximation, as we show in Sec. III C. For small pressure, the symmetric stretching frequency has the expansion,

$$\omega_s(P)\simeq\omega_s(0)(1-\tfrac{1}{2}P/P^*) . \quad (14)$$

This has the interesting consequence that the slope of ω_s acts as a "pointer" to the phase transition pressure P^*. The slope is $-\frac{1}{2}$ if the pressure is measured in P^* units. This simple scheme can be used to *predict* P^* from low-pressure data alone.

In Fig. 5 we plot the pressure-dependent frequency of Eq. (13) along with the experimental data. The theoretical frequency of Eq. (13) has two parameters, $\omega_s(0)$ and P^*. The parameter $\omega_s(0)$ is simply fit to the experimental

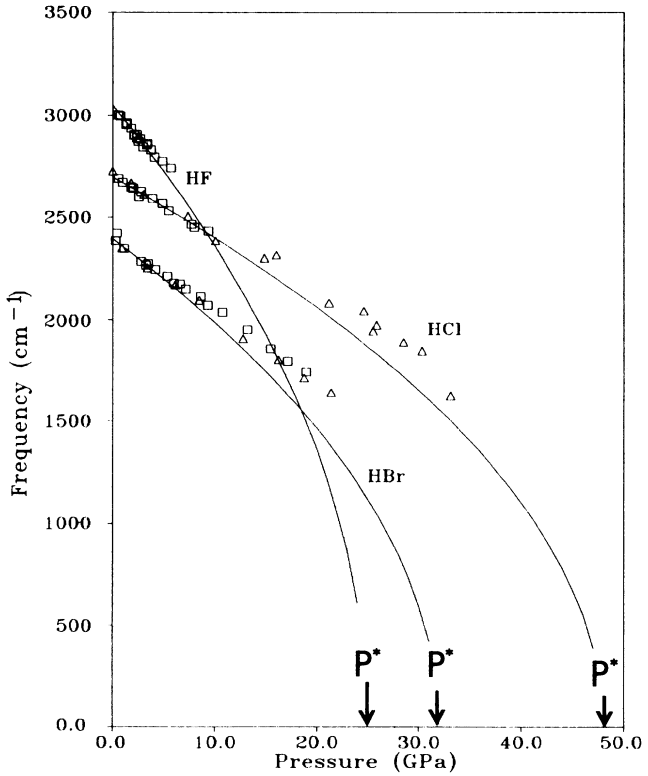

FIG. 5. Experimental Raman scattering A_1-mode frequencies [triangles (Ref. 10) and squares (Refs. 9 and 14)] for HF, HCl, and HBr, compared with the pressure-dependent classical frequencies ω_s of Eq. (13) (solid line). The predicted critical pressure P^*, extrapolated from the low-pressure slope, is shown for HF and HCl.

zero-pressure frequency. For HBr Johannsen *et al.*[10] have reported an experimental observation of the phase transition, so we use their experimental value of $P^*=32$ GPa. Comparing the theoretical and experimental curve for HBr we notice that agreement at low pressures is excellent while deviations occur at higher pressure. This is precisely as expected. At low pressure the barrier is high, and tunneling and other nonlinear behavior are expected to be absent. The linear approximations made in this section ought to be valid here, and indeed the $-\frac{1}{2}$ slope rule is very well obeyed in this region.

For HF and HCl the phase transition to the symmetric hydrogen phase has not yet been seen. Here we use the pressure derivative of the A_1 stretching mode frequency as determined by Raman scattering to predict P^*. In Fig. 5 we show the data of Johannsen *et al.*[10] and Hanson and co-workers[9] for HBr and HCl. We also present new experimental data for the symmetric stretching mode of HF. The data on HF is presently incomplete because of the very weak Raman scattering of this material coupled with interference effects in the diamonds. Our theoretical predictions for P^* in HF ($P^*=25$ GPa) and HCl ($P^*=48$ GPa) are also shown in Fig. 5. To our knowledge, no experiments to check these predictions have been performed on these materials. Promising experiments on HF and DF are currently in progress and will be published separately.[14]

The zone boundary $q=\pi/d$ mode gets zone folded into a zone-center mode for the zigzag chain (4 atoms/cell). This asymmetric stretching (B_2) mode has frequency $\omega_A=[(\Omega_0^2+\Omega_1^2)]^{1/2}$ and involves both the hydrogen-halide potential V and the hydrogen-hydrogen spring constant K. This makes the precise pressure dependence of this mode more difficult to interpret since Ω_0 decreases with pressure and Ω_1 increases with pressure. In any case, this mode is not predicted to go to zero, although it also will soften with pressure.

C. Quantum Hartree approximation

We now study the nonlinear and quantum effects within this simple model on the phase transition and stretching phonon frequency using a many-body quantum-mechanical approach. Our aim is to resolve the discrepancies between the linear (harmonic) theory of Sec. II B and the experimental optic-mode frequencies at high pressure, and to determine whether the conclusion from the classical model that the phase transition is second order is valid. We begin formally by considering the total energy per unit cell of the system,

$$\epsilon_{\rm tot}=\langle\psi\,|\,H\,|\,\psi\rangle/N\ , \tag{15}$$

with the many-body Hamiltonian H,

$$H=\sum_l P_l^2/2m+\sum_l(\Phi_B/b^4)(x_l^2-b^2)^2 +\tfrac{1}{2}\sum_l K(x_{l+1}-x_l)^2 \tag{16}$$

discussed previously. The ground-state total energy $\epsilon_{\rm tot}$ of Eq. (15) can be evaluated approximately with a Hartree-type expansion of the many-proton wave function $|\psi\rangle$ in terms of single-particle wave functions $|\psi_0\rangle$:

$$|\psi(x_1,x_2,\ldots)\rangle=\prod_l|\psi_0(x_l-ld)\rangle\ . \tag{17}$$

Equation (17) is a product of identical single-particle wave functions, which is appropriate for the ground state. This form of the many-particle wave function and the Hamiltonian of Eq. (16) leads to the Hartree self-consistent single-particle equation for ψ_0,

$$[p^2/2m+\Phi_B(x^2-b^2)^2/b^4 +K(\langle x^2\rangle-2x\langle x\rangle+x^2)]\,|\psi_0\rangle=\epsilon\,|\psi_0\rangle\ , \tag{18}$$

where the mean and mean-square values of the position of the hydrogen atom are calculated between the same ground-state single-particle wave function $|\psi_0\rangle$.

The self-consistent solution to Eq. (18) could in principle be obtained by a numerical iteration process. However, since the single-particle equation [Eq. (18)] depends on the two double-well parameters, Φ_B and b, and on the H-H spring coupling constant K, the functional dependence of the solution on these parameters would remain unclear. Instead we employ a variational principle approach to determine the total energy and use combinations of harmonic oscillator functions localized at the two minima $x=\pm b$,

$$\psi_0(x)=(m\omega/\hbar\pi)^{1/4}(Ae^{-m\omega(x-b)^2/2\hbar}+Be^{-m\omega(x+b)^2/2\hbar}) =A\psi_+(x)+B\psi_-(x)\ . \tag{19}$$

with ω, A, and B as variational parameters. The frequency ω is a mean-field or self-consistent phonon frequency. Substituting Eq. (19) into Eq. (15) yields the expression for the total energy,

$$\begin{aligned}\epsilon_{\rm tot}=&(1/2m)(\hbar^2\alpha/2-2ABS\hbar^2b^2\alpha^2)\\ &+(\Phi_B/b^4)[3/4\alpha^2+(A^2+B^2)b^2(3/\alpha+b^2)]\\ &+\left[k-\frac{2\Phi_B}{b^2}\right][1/(2\alpha)+(A^2+B^2)b^2]\\ &-K(A^2-B^2)b^2+\Phi_B\ ,\end{aligned} \tag{20}$$

where $\alpha\equiv m\omega/\hbar$ and S is the overlap integral, $S=\langle\psi_+\,|\,\psi_-\rangle=e^{-\alpha b^2}$. Equation (20) is then minimized with respect to ω, A, and B subject to the normalization condition

$$1=A^2+B^2+2ABe^{-m\omega b^2/\hbar}\ . \tag{21}$$

We first consider the case of zero pressure. As expected, the minimum total energy obtained from Eq. (20) yields the degenerate pair of solutions, $A=1$ and $B=0$, or $A=0$ and $B=1$, indicating the hydrogen eigenfunction is composed only of ψ_+ or ψ_-. This situation is shown in Fig. 6(a) for the case of HBr. Here the hydrogen atom is localized in one of the wells, indicating a well-defined asymmetrically bonded structure.

As pressure is increased the central barrier is reduced rapidly and the wave function spreads out, peaking nearer x equal to zero, the bond midpoint. For nonzero pressure, we use the values of P^* in Eqs. (6), (7), and (8) determined by Fig. 5. At high enough pressure, the hydrogen tunnels into the other well thus altering the symmetry of the

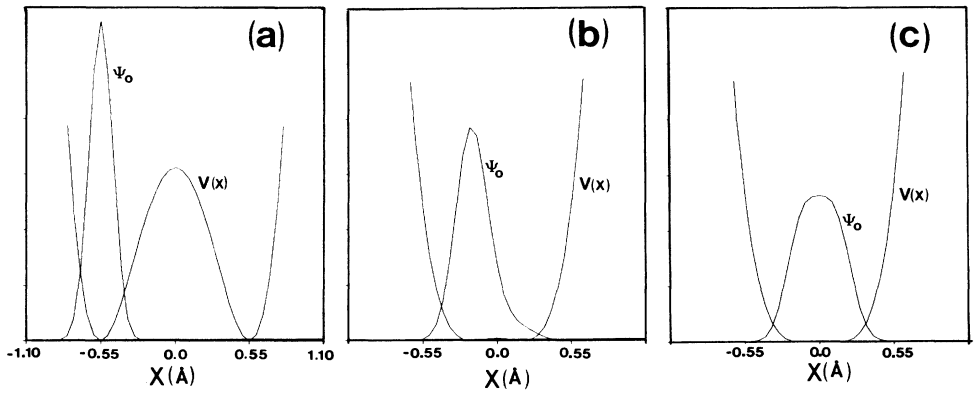

FIG. 6. Ground-state hydrogen wave function for HBr at (a) zero pressure, (b) just under the quantum phase transition P_c, and (c) just above P_c. The bond potential $V(x)$ is also shown.

molecular bond [Fig. 6(b)]. At some quantum-mechanical "critical pressure" P_c, the minimum energy configuration is the symmetric phase ($A=B$), in which the probability density in the left and right wells is equal [Fig. 6(c)]. The pressure P_c is different from the classical critical pressure P^*. For HF, HCl, and HBr we find the quantum critical pressures to be $P_c \simeq 22$, 45, and 30 GPa, respectively, which are only slightly below the classical phase transition pressures $P^*=25$ GPa, 48 GPa, and 32 GPa, respectively. At P_c, the bond potential still exhibits a double minimum, but the barrier is reduced nearly 3 orders of magnitude from that at zero pressure.

We find the transition at P_c to be continuous (second order) as can be seen from Fig. 7. There we show the pressure dependence of the wave function parameters A and B of Eq. (19) for HBr obtained from the variational technique. We consider the system at zero pressure to be in the left ground state in Fig. 7, so that $A=0$ and $B=1$. As the pressure increases, A remains equal to zero until the pressure approaches $\simeq 23$ GPa. Then the hydrogen begins to tunnel and the single-particle wave function begins to receive contributions from both ψ_+ and ψ_-. Finally, at the quantum phase transition pressure P_c, the minimum energy configuration has equal contributions from both ψ_-, and ψ_+ and $A=B$. Although the phase transition is predicted to be second order, it appears to occur over a narrow pressure range.

A comparison of the mean value of the hydrogen position in classical and quantum-mechanical theory is shown in Fig. 8 for HBr. The quantum expectation value $\langle x \rangle_q$ is determined from the wave function of Eq. (19) and yields

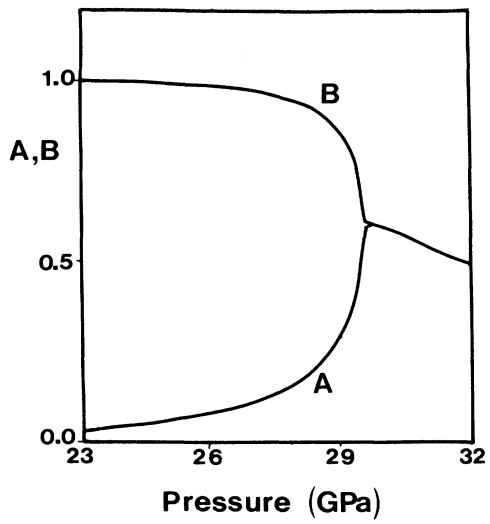

FIG. 7. Wave-function variational parameters A and B of Eq. (19) as a function of pressure for HBr. As A increases, B decreases and the hydrogen atom begins to move from its left ground state towards the center of the bond until at the phase transition pressure ($P_c \simeq 30$ GPA) the symmetric-bond configuration is reached. Note the pressure scale, and that the transition, although second order, occurs rapidly.

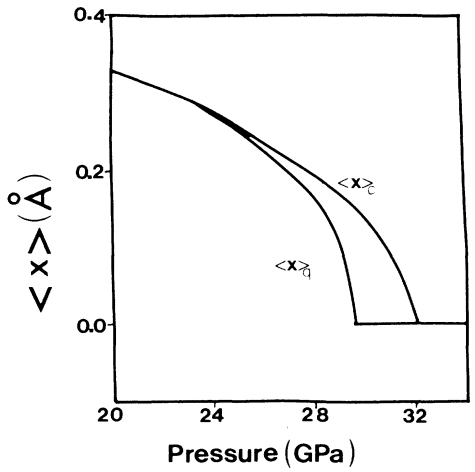

FIG. 8. Comparison between the classical hydrogen position, $\langle X \rangle_c$, and the quantum mean value of the position, $\langle X \rangle_q$, as a function of pressure. The transition to $\langle x \rangle = 0$, symmetric hydrogen, occurs at lower pressure quantum mechanically due to tunneling.

$$\langle x \rangle_q = (B^2 - A^2) b(0) [(1 - P/P^*)]^{1/2} . \quad (22)$$

The classical hydrogen position, $\langle x \rangle_c$, is obtained by placing the atom at its minimum potential energy position;

$$\langle x \rangle_c = b(0) [(1 - P/P^*)]^{1/2} . \quad (23)$$

The quantum and classical results agree in HBr for $P \leq 23$ GPa (see Fig. 8) but deviate at higher pressures due to quantum tunneling.

The quantum nature of these crystals is also evident in the Raman scattering measurements of the A_1 and B_2 vibrational mode frequencies as a function of pressure. In Fig. 9 we compare the classical and quantum theoretical A_1-mode optic-phonon energies with experiment for HBr.[9,10] A precise theoretical calculation of the optic-mode energies requires a difference in total energy of the excited and ground states. Since our Hartree wave function in Eq. (17) is appropriate only for the ground state, we make the additional approximation that the energy difference between excited and ground states is twice the ground-state energy—an exact result for a truly harmonic system. This possibly could be a severe approximation in some cases. Our results involving the excited states should therefore only be taken to be an indication of the size of the quantum effects to be expected from a proper treatment of the excited states. The zero pressure quantum-mechanical energy was fit to experiment by a slight adjustment of the barrier height Φ_B from its classical value. The phonon energies derived from our quantum model agree very well with the experimental data. In particular, the discrepancy present in the classical result at high pressure has been removed. The final increase in energy, at $P > P_c$, is attributed to the increase of the kinetic energy of the hydrogen atom due to its increased confinement.

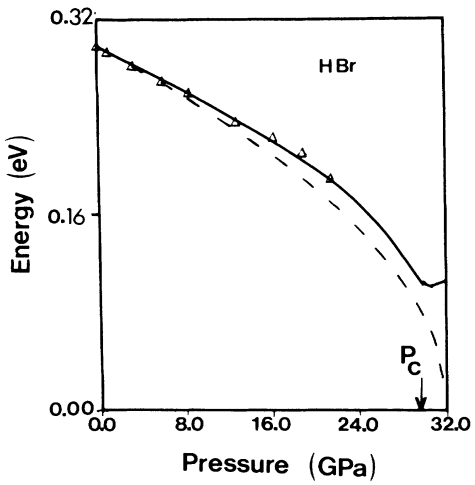

FIG. 9. Comparison of experimental (triangles, Ref. 10), classical theory (dashed line), and quantum theory (solid line) symmetric stretch (A_1) mode energies $\hbar\omega$. The quantum theory removes the discrepency at higher pressures and predicts that the energy will increase past the critical pressure P_c.

Since the quantum behavior of these systems is mainly a consequence of the light hydrogen atom, we expect a significant isotope effect. We find that DBr is symmetrically bonded at a higher pressure ($P_c \simeq 31$ GPa) than HBr ($P_c \simeq 30$ GPa). The deuterium begins to tunnel through the double-well potential barrier at the higher pressure $P \simeq 29$ GPa (versus 23 GPa for HBr) so that the pressure range in which the phase transition proceeds is considerably narrower than that for HBr.

D. Solitons

In the previous sections we have seen how, in order to describe properly the dynamic properties of these materials, we were forced to abandon the harmonic model and to make use of an anharmonic, double-well bond potential. This led to a second-order phase transition under pressure from an asymmetric bonded to a symmetrically bonded crystal. Another possible excitation of these materials involves the transformation of material in the right ground state to the left ground state, i.e., a solitonic excitation.[26–30] This would involve moving some atoms over the barrier Φ_B, an energy which is very pressure dependent and tends to zero at high pressure.

A fully microscopic quantum-mechanical solution of this problem is not possible, so we consider only the classical approximation. We consider the Hamiltonian of Eq. (16), and work in the long-wavelength limit. This amounts to replacing the discrete lattice, $=0,\pm 1, \ldots$, as a continuum where now $x(t)$ is replaced by $x(z,t)$ and z is continuous. The wave equation from Eq. (16) in this approximation is

$$\left[\frac{\partial^2}{\partial z^2} - \frac{1}{c^2} \frac{\partial^2}{\partial t^2} \right] x = \frac{4\Phi_B}{K d^2 b^4} x (x^2 - b^2) , \quad (24)$$

with d being the lattice constant separating two neighboring Br atoms along a linear chair and $c = (Kd^2/m)^{1/2}$ the "speed of sound" derived from the H—H harmonic coupling. The "speed of sound" c is not the true acoustic mode speed of sound, but the speed c appearing in the long-wavelength limit of Eq. (12), $\omega^2 = \Omega_0^2 + c^2 q^2$. Equation (24) has solutions of the form,

$$x(z,t) = x(z - vt) = -b \tanh[(z - vt)/Wd] . \quad (25)$$

The width W is given by

$$W = \frac{1}{\gamma(v)} \left[\frac{\frac{1}{2} k b^2}{\phi_B} \right]^{1/2} , \quad (26)$$

where $\gamma(v) = (1 - v^2/c^2)^{-1/2}$.

A schematic of this wave is shown in Fig. 10. The solution, Eq. (25), represents a localized traveling wave or, more precisely, a traveling "solitary" kink. It is an excitation connecting material on the left in the left ground state to material on the right in the right ground state. The wave travels with velocity v which may be zero. In fact v is arbitrary except $v < c$. Other shapes can be constructed by adding the partner solution which connects the right ground state on the left to the left ground state on the right. The hydrogen halides are an extremely important candidate for the study of solitons since (i) the

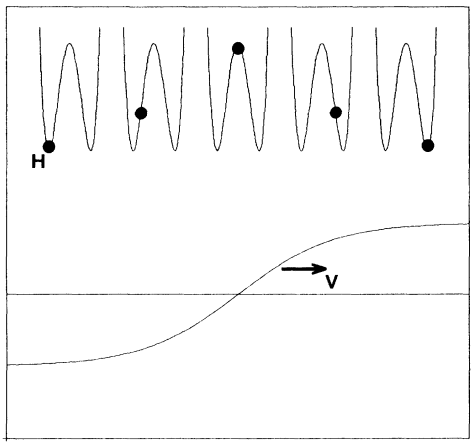

FIG. 10. Schematic diagram of the kink soliton in a solid hydrogen halide. The upper diagram shows the position of the light hydrogen atom in their double well potential between two heavy halides. The leftmost H atom is in the "left" ground state, and the rightmost H atom is in the "right" ground state. The kink soliton given by Eq. (25) is plotted at the bottom of the diagram. It propagates through the crystal with velocity v, and connects the two degenerate ground states.

materials form a relatively simple lattice and (ii) as we now show, the nonlinearities are easily tuned by pressure.

Let us see how the energy of the soliton is expected to vary with pressure. The kinetic energy is

$$T=\tfrac{1}{2}mv^2\gamma(v)\left[\frac{4}{3}\frac{b}{d^2}\left[\frac{2\phi_B}{K}\right]^{1/2}\right]\simeq T_0(1+O(v^2/c^2)) , \tag{27a}$$

and the potential energy is

$$V=\tfrac{1}{2}Kd^2\left[\frac{4b}{3d^2}\left[\frac{2\phi_B}{K}\right]^{1/2}\right]\left[\gamma+\frac{1}{\gamma}\right]$$

$$\simeq V_0+O(v^4/c^4) . \tag{27b}$$

The approximate form of these equations is for small velocities. At zero velocity, the minimum energy to create a soliton is $V_0=\frac{8}{3}(\frac{1}{2}Kb^2\phi_B)^{1/2}$. The pressure dependence of the width W and minimum energy of formation are

$$W(P)=W(0)(1+\tfrac{1}{2}P/P^*)^{1/2}(1-P/P^*)^{-1/2}$$

and

$$V_0(P)=V_0(0)(1+\tfrac{1}{2}P/P^*)^{1/2}(1-P/P^*)^{3/2} .$$

Thus W and V_0 depend critically on pressure with $W\to\infty$, and $V_0\to 0$ at the phase transition. Estimates for $W(0)$ and $P(0)$ based on our calculations of HBr given in Sec. III and those of HF give $W(0)\simeq 0.5d$ and $V_0(0)\simeq 1-3$ eV. The energy associated with soliton formation at low pressures is relatively high and thus can only be created with high energy probes. However, at high pressure the formation energy decreases dramatically and they may be created thermally. As the phase transition is approached, the formation of solitons may be the driving mechanism in the fluctuations of the hydrogen positions.

Solitons can form in this model at any pressure. However, as pressure increases, the interaction between chains becomes stronger, and the model needs to be extended. For instance, the solitonic states may need to be soliton-antisoliton pairs to keep the energy finite when interchain interactions are strong. Theoretical studies on polyacetylene[31,32] have considered chain-chain interactions and have predicted the formation of soliton superstructures.[31] The simple single soliton discussed here is, in any case, a building block for a more complete theory.

III. *AB INITIO* ELECTRONIC STRUCTURE CALCULATION FOR HBr

In this section we describe our *ab initio* local-density approximation (LDA) calculation of the electronic states and total energy for one particular hydrogen halide, HBr. These calculations are able to predict entirely from first principles the optic-mode frequency and the transition to the symmetric phase, and can be used to test some of the assumptions made to construct the simple model of Sec. II. In Sec. IV we discuss similar calculations for H_6F_6 rings using the Hartree-Fock approximation.

We first briefly review the LDA and justify our use of this approximation for the case of HBr and in particular for hydrogen. Next we describe the construction of the pseudopotentials for Br used in our calculation. Finally, we discuss our results for the total energies and electronic states of a linear form of HBr in both the symmetric and asymmetric phases.

A. Local-density approximation

Hohenberg and Kohn[33] and Kohn and Sham[34] showed that the ground-state energy of an inhomogeneous electron gas in the potential of the ions $V_{\rm ion}(r)$ is a unique functional of the electron density $n(r)$. Assuming that $n(r)$ is sufficiently slowly varying, Kohn and Sham[34] derived the local-density approximation (LDA) of the total electronic energy,

$$E_e^{\rm LDA}(n)=T[n]+\int V_{\rm ion}(r)n(r)d^3r+\frac{e^2}{2}\int\int\frac{n(r)n(r')}{|r-r'|}d^3r\,d^3r'+\int n(r)\varepsilon_{\rm xc}(n(r))d^3r . \tag{28}$$

Here $T[n]$ is the kinetic energy and $\varepsilon_{\rm xc}(n)$ is the exchange-correlation energy functional. Writing n as a sum over occupied single particle orbitals ψ_i, and minimizing Eq. (28) with respect to variations of ψ_i yields the Schrödinger-type equation for the single electron states,

$$\left[\frac{p^2}{2m}+V_{\text{ion}}(r)+e^2\int d^3r'\frac{n(r')}{|r-r'|}+\mu_{\text{xc}}(n(r))\right]\psi_i(r)=E_i\psi_i(r)\ . \tag{29}$$

The terms are the kinetic energy, electron-ion interaction, electron-electron Hartree repulsion, and the exchange-correlation potential,

$$\mu_{\text{xc}}(n)=\frac{d}{dn}[n\varepsilon_{\text{xc}}(n)]\ .$$

The exchange-correlation energy is broken up into an exchange term and a correlation term, $\varepsilon_{\text{xc}}(n)=\varepsilon_{\text{x}}(n)+\varepsilon_{\text{c}}(n)$. The exchange potential of the free-electron gas is

$$\varepsilon_{\text{x}}(n)=-\frac{3e^2}{4}\left[\frac{9}{4\pi^2}\right]^{1/3}r_s^{-1}=-\frac{0.916\ \text{Ry}}{r_s/a_0}\ , \tag{30}$$

where $n=(\frac{4}{3}\pi r_s^3)^{-1}$ and a_0 is the Bohr radius. In the high-density limit ($r_s\to 0$), Gell-Mann and Brueckner[35] find the correlation energy

$$\varepsilon_c=(e^4m/2\hbar^2)[(2/\pi^2)(1-\ln 2)\ln(r_s/a_0)-0.096+O(r_s)]\ .$$

In HBr the average density r_s is $\simeq 2.4a_0$. A number of interpolation formulas for ε_c exists in the literature for large and intermediate r_s. We use the Monte Carlo results of Ceperley and co-workers[36,37] as parametrized by Perdew and Zunger,[38]

$$\varepsilon_c=\begin{cases}\dfrac{0.2846}{1+1.059[(r_s/a_0)]^{1/2}+0.3334(r_s/a_0)}\ \text{Ry}, & r_s/a_0>1\\ [0.0622\ln(r_s/a_0)-0.0960+0.0040(r_s/a_0)\ln(r_s/a_0)-0.0232(r_s/a_0)]\ \text{Ry}, & r_s/a_0<1\ .\end{cases} \tag{31}$$

We now briefly discuss the use of the LDA for hydrogen. Since hydrogen has only one electron in a relatively compact orbital, it might be expected that the local density approximation fails for this atom. In the LDA, the single electron is allowed to interact with itself via its own Coulomb field, and to correlate with itself. However, as shown by Gunnarson *et al.*[39], the errors due to the LDA for hydrogen are no larger than for other atoms if the fact that the spin is unpaired and the exchange-correlation energy for a spin polarized electron gas is used.

To see the origin of the difficulties, and their resolution, consider a trial wave function for the hydrogen ground state of the form $\psi=e^{-r/a}/(\pi a^3)^{1/2}$, which is the same as the exact wave function except that a is considered as a variational parameter. The expectation value of the energy can then be evaluated analytically in the LDA if we replace the exchange-correlation energy given by Eqs. (30) and (31) by the simpler Slater form

$$\varepsilon_{\text{xc}}(n(r))=-(\alpha 9e^2/8\pi)[3\pi^3n(r)]^{1/3}\ , \tag{32}$$

where α is $\frac{2}{3}$ for the exchange only. Typically α is chosen between $\frac{2}{3}$ and 1 which includes correlation effects in an average way. The total electronic energy using Eq. (28) is,

$$\begin{aligned}E_{\text{tot}}&=NT+NU_{\text{ion}}+N^2U_{\text{ee}}+N^{4/3}U_{\text{xc}}\\&=N\hbar^2/2ma^2-Ne^2/a+\tfrac{5}{16}N^2e^2/a\\&\quad-N^{4/3}(0.319\alpha e^2/a)\\&=N[\hbar^2/2ma^2-Z^*(N)e^2/a]\ ,\end{aligned} \tag{33}$$

where the four terms are the kinetic, electron-ion, electron-electron, and exchange-correlation energies. The quantity N is the occupation number of the orbital which is 0, 1, or 2 for H^+, H^0, and H^-, respectively. The quantity $Z^*(N)$ $[=1-\frac{5}{16}N+N^{1/3}(0.319)\alpha]$ acts as an effective charge for the hydrogen atom.

The total energy in Eq. (33) has two errors; the electron interacts with itself and exchanges with itself. Perdew and Zunger[38] have proposed corrections to these self-interactions, which in this case amount to the removal of these two terms. Without their removal, however, one sees that these two terms tend to cancel. Minimizing the total energy in Eq. (33) with respect to a yields $E_{\text{tot}}=-NZ^{*2}$ Ry. For the present we consider the one electron hydrogen atom, $N=1$. The value of Z^* is then 1.01 and 0.90 for α equal to 1 and $\frac{2}{3}$, respectively. The total energy is then -1.01 Ry and -0.81 Ry, respectively. These analytic results bracket from above and below the numerical result of -0.89 Ry obtained by integrating the radial equation using the exchange-correlation energy of Eqs. (30) and (31).

The 11% error in the total energy for the numerical solution of the hydrogen atom in LDA can be reduced to 2% when polarization effects are taken into account. For a He atom, where the spins are compensated, the error for the total energy in the LDA using the exchange-correlation energy of Eqs. (30) and (31) is found to be 2.3%. For the hydrogen halides, which are wide-band-gap insulators, the spins are paired and we expect the errors due to hydrogen to be no worse than for other atoms.

One remaining difficulty of the LDA which applies not only to H, but also to the halides F, Cl, and Br as well, is that the negative ions H^-, F^-, Cl^-, and Br^- are all experimentally stable, while the LDA finds that they are

not[40,41] (see Fig. 11). Our calculations of solid HBr described in Sec. III show, however, that hydrogen, and therefore Br, are roughly neutral atoms. Thus the instability of the negative ions is not an important consideration in our work, at least in HBr.

B. Br pseudopotential

The Br pseudopotentials were constructed following the method of Hamann, Schluter, and Chiang.[42] The pseudo—wave functions fit the true (full core) wave functions outside a radius $r_{\rm cut}(l)$. The full core and pseudoatomic wave functions for the s and p orbitals of Br in the s^2p^5 configuration are shown in Fig. 12. The values of $r_{\rm cut}(l)$ chosen were $r_{\rm cut}(l)/r_{\rm peak}(l)=1.3$, 1.3, and 1.5, for s, p, and d wave functions respectively, where $r_{\rm peak}(l)$ is the radius of the outermost peak in the full core wave function. We found this cutoff was accurate, yet soft enough to be useful in a calculation which uses a finite plane-wave basis. The s- and p-ionic pseudopotentials for Br [Fig. 12(c)] were produced from the ground state s^2p^5 configuration. The d pseudopotential was produced from the $s^1p^{3.75}d^{0.25}$ configuration which keeps the d wave function somewhat confined.

The ionic pseudopotentials were then fit to analytic functions for computational convenience. Good fits were obtained using the functional form of Bachelet *et al.*[43] The pseudopotentials (in atomic units) are split into a long-range, angular momentum independent core potential $V_{\rm core}(r)$,

$$V_{\rm core}(r)=-Z_v/r\left[\sum_{i=1,2}c_i\,{\rm erf}[(\alpha_i^{\rm core})^{1/2}r]\right], \tag{34}$$

where Z_v denotes the valence charge and c_i and $\alpha_i^{\rm core}$ are fitting parameters, and a short range angular momentum dependent potential $V_l(r)$

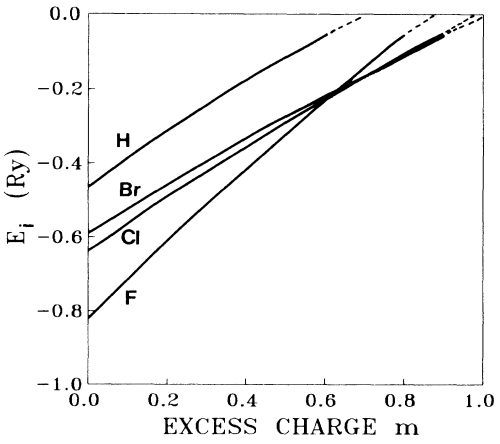

FIG. 11. Plot of the energy eigenvalue E_i for the outermost valence electron for the negatively charge ions H^{-m}, Br^{-m}, Cl^{-m}, and F^{-m}. The exchange correlation used is given in Eqs. (30) and (31). The appearance of positive eigenvalues indicates an unbound system.

$$V_l(r)=\sum_{i=1,3}[A_i(l)+r^2A_{i+3}(l)]e^{-\alpha_i(l)r^2}, \tag{35}$$

where l is the angular momentum s, p, or d. The core parameters c_1 and c_2 satisfy the condition $c_1+c_2=1$.

Since $V_{\rm core}(r)$ is not uniquely defined, a simple procedure involving only small exponents, was used to obtain the remaining three core parameters. In this method the three core parameters c_1, $\alpha_1^{\rm core}$, and $\alpha_2^{\rm core}$ are uniquely determined by the simple boundary conditions, (i)

$$V_{\rm core}(r_{\rm cut}^{\rm av})=-Z_v/r_{\rm cut}^{\rm av},$$

(ii)

$$V_{\rm core}(0)=-(Z_v/r_{\rm cut}^{\rm av})Q,$$

and (iii)

$$\lim_{r\to0}\left[-Z_v\left[c_1\frac{{\rm erf}[(\alpha_1^{\rm core})^{1/2}r]}{r}\right]\right]=-(Z_v/r_{\rm cut}^{\rm av})P,$$

where $r_{\rm cut}^{\rm av}=\frac{1}{3}[r_{\rm cut}(s)+r_{\rm cut}(p)+r_{\rm cut}(d)]$. Condition (i) is imposed to guarantee that the potential must be nearly equal to $-Z_v/r$ for r greater than $r_{\rm cut}^{\rm av}$. Condition (ii) simply enables one to adjust the potential at the origin to a reasonable value; a factor of Q ($\simeq$2—3) times that at $r_{\rm cut}^{\rm av}$. The last condition, (iii), ensures by adequate choice of P that the core pseudopotential is smooth. This procedure leads to a transcendental equation which is easily solved numerically. Solutions were found when Q and P satisfied $Q<P$ and $Q>1$, and were chosen to be 2 and 4, respectively.

The remaining potential $V_l(r)$ was fit by a least-squares procedure for several choices of exponential factors $\alpha_i(l)$. The six $A_i(l)$ parameters for each choice of $\alpha_i(l)$ are determined through the inversion of a 6×6 matrix. All of the fitting parameters are listed in Table I.

C. *Ab initio* calculation for HBr

We have computed the electronic states and total energy of HBr in the LDA using a linear chain form of solid HBr. The geometry of this linear form is simplified from the base-centered-orthorhombic "kinked-chain" structure

TABLE I. Coefficients and decay constants for the core [Eq. (34)] and angular-momentum-dependent [Eq. (35)] pseudopotentials for Br. We use atomic units.

i	1	2	3
$\alpha_i^{\rm core}$	1.69	1.35	
$c_i^{\rm core}$	2.270	−1.270	
$\alpha_i(s)$	1.73	1.91	3.53
$A_i(s)$	−16 830.8403	16 712.4864	128.0605
$A_{i+3}(s)$	1219.0349	1952.9406	71.7046
$\alpha_i(p)$	1.82	2.09	4.07
$A_i(p)$	4047.0411	−4004.3060	−35.6983
$A_{i+3}(p)$	−458.3421	−675.2193	−25.8234
$\alpha_i(d)$	2.04	2.77	4.03
$A_i(d)$	921.5252	−524.7374	−390.0447
$A_{i+3}(d)$	−209.6522	−763.9507	−181.2859

of Fig. 1, to the base-centered-tetragonal "straight-chain" structure shown in Fig. 4. This simplification is motivated by the fact that the hydrogen and covalent bonds along the chain are more important (at least as far as the hydrogen atom is concerned) than interchain bonding. The important practical simplification of the linear structure is that it has reduced the number of geometric parameters to three compared with five in the zigzag chain. Variations of five geometric parameters to find the minimum energy configuration was judged to be impractical, and would add little physical insight into the problem. Furthermore, the linear chain has increased the number of available group operators, an additional simplification. The three geometrical parameters (see Fig. 4) are the chain-chain lattice constant a, the Br-Br intrachain distance d, and the fractional hydrogen position τ [$\equiv d_{\text{H-Br}}/(d/2)$]. We have fixed the lattice parameter a to the value $a=5.78$ Å, which is the average of the two different interchain lattice constants (a and b) of the original base-centered-orthorhombic crystal.

The total energy for a given geometric configuration (τ,d,a) is computed using the self-consistent pseudopotential momentum space formalism of Ihm, Zunger, and Cohen.[44] The total energy is written as

$$E_{\text{tot}}(\tau,d,a)=T(\{\tau,d,a\})+\sum_{\mathbf{g}} V(\mathbf{g};\{\tau,d,a\}) +C(\{\tau,d,a\}) ,$$

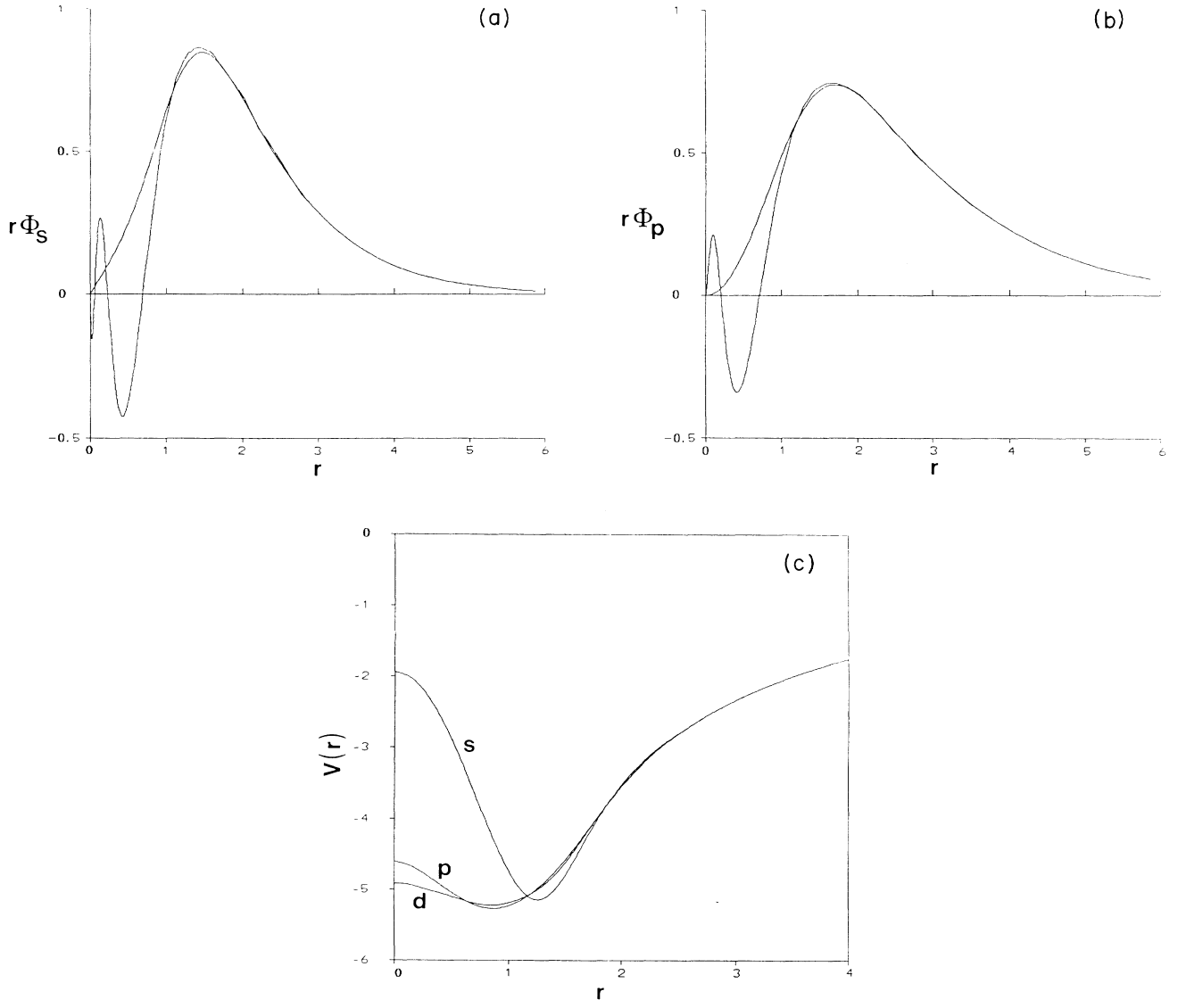

FIG. 12. Comparison of the (a) pseudo-s wave functions and (b) p wave functions of Br with the full core wave functions. (c) shows the s-, p-, and d-Br pseudopotentials. The pseudopotentials are norm conserving and the pseudo—wave functions are identical to the full core wave functions in the tail region. Atomic units are used.

where T is the kinetic energy, C is a lattice-dependent quantity which is independent of the valence charge density and $V(\mathbf{g};\{\tau,d,a\})$ depends on the valence charge density and includes the Fourier transform for reciprocal lattice vector $\mathbf{g}$ of the electron-ion and electron-electron interactions. We use four special $\mathbf{k}$ points to perform the sum over the irreducible wedge of the Brillouin zone, and use a plane-wave basis which includes plane waves with kinetic energy up to 140 eV ($\simeq$10 Ry). The pseudopotential described in Sec. III B was used for the seven valence electrons of Br, while we use the full core potential ($1/r$) and not a pseudopotential for hydrogen.

The band-structure energies $E_{n,k}$ and wave functions are determined from the Schrödinger-type single particle Eq. (29). We show in Fig. 13 the band energies $E_{n,k}$ for the three cases: (a) Zero-pressure Br-Br distance d (3.91 Å) with H *symmetric* ($\tau=\frac{1}{2}$) between Br, (b) zero-pressure Br-Br distance d (3.91 Å) with H at its *asymmetric* minimum energy configuration ($\tau=0.75$), and (c) H at the symmetric position ($\tau=1.0$) with the Br-Br distance $d=3.21$ Å which is near the predicted phase transition. The four lowest bands are occupied by electrons, and the material is an insulator for all cases shown. The lowest five bands, starting from lowest energy, correspond to s(Br), a bonding band between sp_σ(Br) and s(H), a pair of bonding p_π(Br) bands, and an antibonding sp_σ(Br) and s(H) band. Here the p_π orbital is perpendicular to the chain, and the p_σ is along the chain. Notice that the p_π and s(Br) are little affected by Br-Br distance d or H position τ. Large changes occur only in the sp_σ(Br)—s(H) bonding and antibonding bands. Note in particular at zero pressure [$d=3.91$ Å, Figs. 13(a) and 13(b)], the bonding-antibonding gap more than doubles when H is moved to its equilibrium off-center position. The sp_σ(Br)—s(H) bands also become narrower for asymmetric H, since the bonding is mainly between the HBr molecular units and is less cooperative. Also, for asymmetric hydrogen the occupied bonding sp_σ(Br)—s(H) bond is lowered in energy overall leading to the asymmetric configuration being the lower energy state.

At the phase transition [Fig. 13(c)], the bonding sp_σ(Br)—s(H) has "punched" through the p_π bands, so that the direct gap at Γ has changed character. The bonding-antibonding sp_σ(Br)—s(H) gap has been reduced from $\simeq$7 eV at zero pressure to about half that at the phase transition. However, the material is still an insulator, and an insulator-metal phase transition has not yet occurred.

The character of the bonding can be seen from the charge-density contour plot shown in Fig. 14. In this figure we show the charge-density contours computed self-consistently for $d=3.91$ Å (zero pressure) with (a) H at the symmetric position ($\tau=1.0$) and (b) at the asymmetric minimum energy position ($\tau=0.75$). As can be seen, there is very little interchain interaction in either the symmetric or asymmetric phase, with the charge being used to form bonds along the chains. Within the chains we see that, as the hydrogen goes from the symmetric to the asymmetric phase, an extra peak in the charge-density forms corresponding to the formation of the HBr covalent molecular bond. These "pear-like" charge densities in the asymmetric phase have a slight overlap from one molecule to its neighbor due to the hydrogen bond.

Moving the hydrogen to the symmetric position [Fig. 14(a)] causes the charge density to spread out more and the covalent bonding peak is lost. Unlike an alkali atom in the (symmetric) alkali halides, the hydrogen atom refuses to give up its electron and form an ionic solid. The

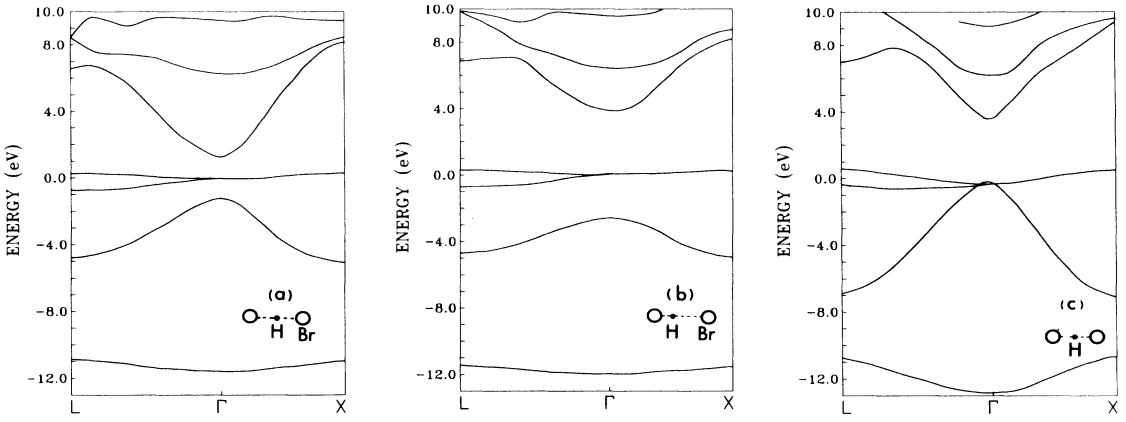

FIG. 13. Band structure for solid HBr from the *ab initio* LDA method described in Sec. III. The lowest five bands are the s(Br), sp_σ(Br)—s(H) bonding, two p_π(Br) bonding and sp_σ(Br)—s(H) antibonding bands. (a) and (b) show symmetrically (a) and asymmetrically (b) bonded hydrogen at zero pressure (or $d=3.91$ Å). In asymmetric phase (b) the energy is minimum and the atoms form H-Br covalently bonded molecular pairs with very little interactions between the pairs so that the bands are relatively flat. In the symmetric state, however, the hydrogen interacts equally with both of its neighboring halide atoms so that the dispersion in the bands is increased from that of the asymmetric phase. Past the phase transition pressure ($d=3.21$ Å) to the symmetric phase (c), we find the band width has increased dramatically from its zero pressures values. Note in (c) that the sp_σ(Br)—s(H) bonding band has "punched" through the pressure insensitive p_π(Br) bonding bands giving the band structure a totally new character.

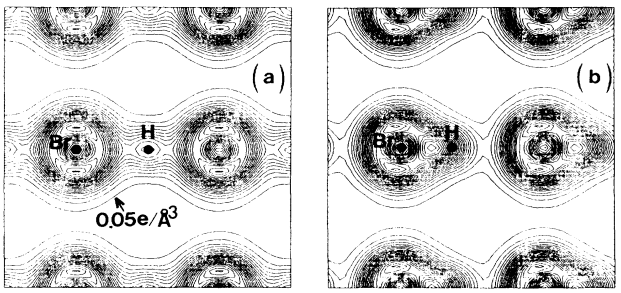

FIG. 14. Topological map of the charge density of HBr at zero pressure in (a) the symmetric state and (b) the asymmetric phase. The lines of constant charge density are separated by $0.05(-e)/\text{Å}^3$. We find very little interchain interaction in either phase so a linear chain model appears to be reasonable. The charge localized on the hydrogen atom in either phase is approximately unity. The ground state is (b) where the hydrogen covalently bonds predomenently to one of the Br atoms to form a molecular chain. (b) shows three types of bonding: van der Waals (interchain), hydrogen (intermolecular), and covalent (intramolecular).

charge density around hydrogen is significant; in fact, going perpendicular to the chains it is very close to $e^{-2r/a_0}(\pi a_0^3)$.

We now consider the potential energy of the system when we move all hydrogen atoms in unison. This was represented in the model of Sec. II by Eq. (1). We compute the total energy of the system keeping the Br-Br distance fixed at the experimentally observed value, $d=3.9$ Å, and move the hydrogen between them by varying τ. The results are shown in Fig. 15. The results are fit to the two-parameter form of Eq. (1). The value of the barrier height is $\Phi_B=0.6$ eV and the asymmetric displacement $b=0.50$ Å, in good agreement with the experimental value of 0.57 Å. We see that the fit of the simple model potential of Eq. (1) to the *ab initio* LDA calculation is nearly perfect. This suggests that the complicated bonding mechanisms of these systems can be understood in the simple terms of our model of Sec. II.

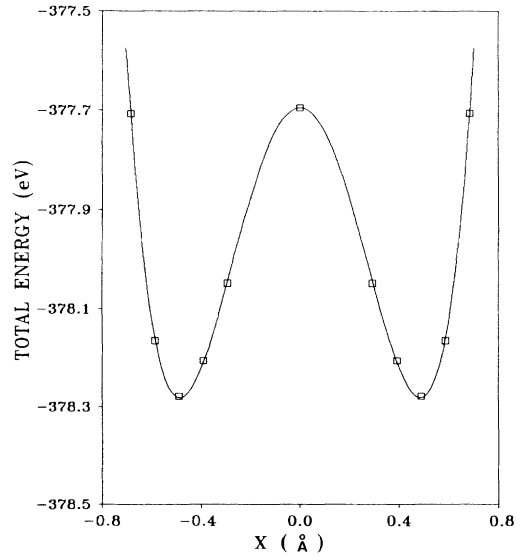

FIG. 15. HBr self-consistent LDA pseudopotential calculation (boxes) verses the model potential $\Phi_B(x^2-b^2)^2/b^4$ fit (solid line).

Experimentally the symmetric stretch optic mode frequency is 2395 cm^{-1} or 0.298 eV. Since this is substantially less than the barrier height Φ_B (0.6 eV), we use a harmonic approximation to determine the frequency theoretically. From the results of Fig. 15 we find 2335 cm^{-1} or 0.290 eV, in excellent agreement with experiment. Based on the fact that theory and experiment for b agree to only within 12%, and that we make the harmonic approximation the extremely small difference in the optic-mode frequencies is probably somewhat fortuitous. To include anharmonic effects, we have numerically solved for the single-particle states of the double well given by Eq. (1). The approximate levels of the "left" or "right" states are taken to be the average of a pair of tunnel split states. In this "average tunnel split approximation," the transition frequency is then determined by the difference in magnitude between the average of the lowest pair of levels and the next highest pair. This procedure is expected to be accurate for high barriers (i.e., low pressure). The result is then 2076 cm^{-1} which is within 14% of experiment.

From the considerations of Sec. II C, we expect sizeable corrections to the harmonic approximation as the system approaches the phase transition. Our *ab initio* calculations show this to be correct; in particular, the barrier separating the left and right ground state is very sensitive to the Br-Br chain distance. This is shown in Fig. 16, where the hydrogen potential function is plotted from $d=3.91$ Å (zero pressure) to past the phase transition ($d=3.21$ Å). Note how the curve changes continuously from being concave downward at $x=0$ to being concave upward as pressure is increased. The curves shown in this figure are fits to the analytic form of Eq. (1). The fit in all cases was of equal quality to that of Fig. 15. Past the phase transition $b\rightarrow ib$ [see Eq. (7)].

The total energy as a function of the chain Br-Br distance d and fractional hydrogen position τ is shown in Fig. 17. The global minimum energy occurs very near the observed value of d of 3.91 Å. At this value of d, the minimum energy occurs for $\tau\simeq 0.75$, and the symmetric phase ($\tau=1.0$) lies 0.6 eV above. Reducing the value of d, raises the minimum energy slowly at first, then very rapidly for $d\lesssim 3.5$ Å. The initially soft crystal, becomes stiff appreciably before the phase transition, which occurs at $d\simeq 3.25$ Å. Concomitant with this reduction in d is an increase in the value of τ toward 1, the phase transition value. This rate of increase in τ corresponds to a *stretching* of the bond between hydrogen and its neighboring Bromine, and a *decrease* in the parameter b, which is the distance from the Br-Br center to hydrogen. As d decreases, the minimum energy value of τ changes slowly for d values corresponding to zero pressure and rapidly near the phase transition. This yields small changes in b near zero pressure and rapid changes near the phase transition, and is qualitatively similar to the simple dependence predicted using the pressure variable in Eq. (7).

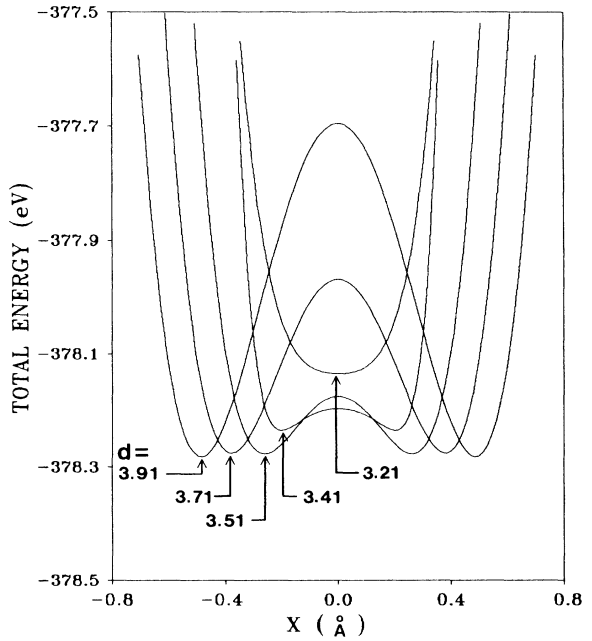

FIG. 16. Total energy as a function of hydrogen position (X) for several choices of the Br-Br displacement ($d=3.21$–3.91 Å). As pressure is increased (d decreased) the central barrier reduces rapidly until at $d=3.21$ Å a critical pressure has been reached and the system has undergone a phase transition to the symmetric phase.

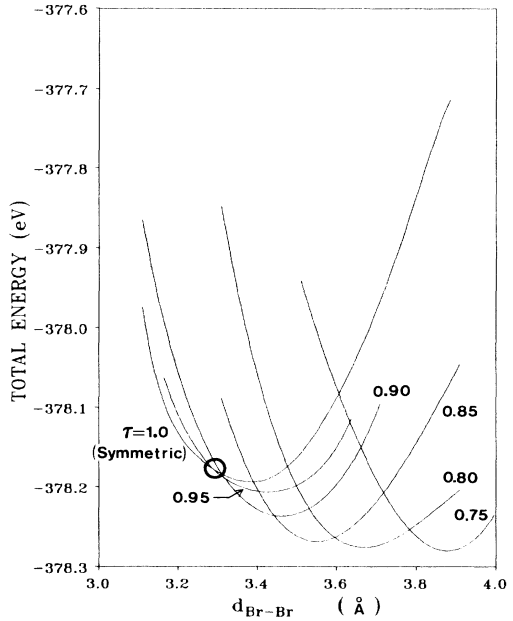

FIG. 17. Total energy as a function of Br-Br distance $d_{\text{Br-Br}}$ within the chain for fixed values of τ from the asymmetric ground-state configuration ($\tau=0.75$) to the symmetric phase ($\tau=1.0$). The ground-state energy is very insensitive to the changes in τ around $\tau=0.75$ but eventually ($\tau=0.90$) the total energy begins to "feel" the potential due to small changes in τ. The system undergoes a phase transition to the symmetric phase ($\tau=1$) around the circled region.

IV. SELF-CONSISTENT FIELD (SCF) CALCULATIONS ON H_6F_6—A MOLECULAR MODEL FOR SOLID HF

In the case of HF, a molecule was chosen that has local geometry very similar to that in the crystal. It is well known that the effect of electron correlation is small on calculated properties such as dissociation energies of the oligomers of HF (Ref. 45) or of processes such as $HF_2^- \rightarrow HF + F^-$.[46,47] We are then fairly sure of arriving at a good representation of the energetics of displacing H atoms at the SCF level. On the other hand, to avoid basis set superposition errors one needs a fairly large basis set with at least one set of polarization functions.[48] We have employed the widely used 6-31G^* (Ref. 49) which has a

TABLE II. Comparison between theory and experiment of lattice constants, optic mode frequencies, total energies, and dissociation energies at zero pressure. Here ω_s is the symmetric stretch (A_1 mode) frequency and ω_A is the asymmetric stretch (B_2 mode) frequency. We compare the frequencies derived using the harmonic approximation with those derived using the "average tunnel split approximation" for a single fourth power potential. To determine ω_A (fourth power) we assumed $\omega_s-\omega_A$ was the same as that found in the harmonic approximation.

	H_6F_6[a]	$(HF)_\infty$[b]	Solid HF (expt)
d(H—F) (Å)	0.901	0.918	0.97[c]
d(F · · · F) (Å)	2.546		2.50[c]
ω_s (harmonic)	3947	3967	3045[d]
ω_A (cm^{-1})	4192	4169	3386[d]
ω_s (fourth power)	3377		3045
ω_A (cm^{-1})	3622		3386
E(SCF) (hartrees)	−100.0256		
ΔE (kJ mol^{-1})	36.5	27.2	

[a]This work.
[b]Reference 18.
[c]References 4 and 5.
[d]Reference 8.

TABLE III. Parameters of the fourth power potential [Eq. (4)] and total energies per HF unit for the H_6F_6 molecular ring in hartree and Å units. The barrier height ϕ_B (in eV) and asymmetric displacement b (in Å) [Eq. (1)] derived from A and D as a function of F · · · F distance are also listed.

d(F · · · F) (Å)	$100+C_s$ (hartrees)	A (hartrees/Å^2)	D (hartrees/Å^4)	$\phi_B=A^2/4D$ (eV)	$b=\sqrt{A}/2D$ (Å)	d(H-F) (Å)	$100+E_m$ (hartrees)
2.700	0.024 69	−0.5460	1.4929	1.36	0.428	0.916	−0.025 01
2.546	0.005 00	−0.5033	2.0601	0.84	0.350	0.921	−0.025 59
2.400	−0.009 53	−0.4217	2.9018	0.42	0.270	0.930	−0.024 70
2.200	−0.016 72	−0.1849	4.8278	0.05	0.138	0.963	−0.018 46
2.150	−0.014 87	−0.0919	5.5297	0.01	0.091	0.984	−0.015 25
2.100	−0.010 99	0.0201	6.3547			1.050	−0.010 99
2.000	0.004 38	0.3159	8.4734			1.000	0.004 38

core function represented by six Gaussians and a split valence function represented by three and one Gaussians, respectively. There are in addition d-like polarization functions on F and p polarization functions on H. With this basis set for HF one finds for the bond length in HF, d(H—F)=0.901 Å (observed 0.917 Å); for the harmonic frequency, $\omega_e=4491$ cm^{-1} (observed $\omega_e=4139$ cm^{-1}); and for the SCF energy −100.0117 hartrees.

The molecule chosen to model the crystal is H_6F_6 with $6/m$ (C_{6h}) symmetry and with the H atoms placed along the F · · · F line. This resembles the geometry found within experimental error in the crystal.[4] The F · · · F · · · F angle of 120° is also very close to that observed in the crystal. The geometry was optimized subject to the constraint that the H atom lay on the F · · · F line. We compare in Table II our calculated values with the results of Beyer and Karpfen[18] who performed SCF calculations for a bent one-dimensional crystal using a somewhat larger basis set than ours, and with experimental results for solid HF. In Table II E is the energy per HF unit and ΔE is the energy to break a H bond, i.e., the energy of dissociation to monomer. The symmetric and asymmetric zone center H—F stretching frequencies were calculated in the harmonic approximation in good agreement with the results of Beyer and Karpfen (BK).

The energy as a function of the displacement of H was also found to be accurately given by a fourth power potential as shown in Fig. 18. We also calculated the frequency of the symmetric mode using the "average tunnel split approximation" of Sec. II C and derived the frequency of the asymmetric mode by assuming that the difference from the symmetric frequency was the same as in the harmonic case. The results are in excellent agreement with the frequencies observed in the crystal[50] suggesting that our molecule does indeed model the crystal rather well. The fact that we get a higher energy for dissociation to monomer than BK is indicative of basis set superposition error as the value estimated from thermodynamic data is 27.5 kJ mol^{-1}.[51] However, as we are primarily concerned with the energy as a function of hydrogen position in the molecule, such errors appear to be relatively unimportant.

The parameters of the fourth power potential are listed in Table III for energies in hartrees per unit HF and distances in Å. Also listed is the minimum energy H—F bond length and the energy E_m at that configuration. From the parameters we can obtain the barrier height ϕ_B and the asymmetric displacement b by comparing Eq. (4) with Eq. (1). The results for ϕ_B and b are shown in Table III. As can be seen the barrier ϕ_B is very sensitive to pressure while the asymmetric displacement b varies more slowly in agreement with the qualitative predictions of Eqs. (6) and (7).

The nature of the phase transition may also be visualized by Fig. 19(a) and by the contour of Fig. 19(b) which plot the total energy for an H_6F_6 ring as a function of the hydrogen displacement x from the symmetric position and d(F · · · F). Figure 19(a) can be compared to the similar Fig. 16 for HBr. These figures clearly demonstrate the cooperative relationship which exists between the hydrogen and the halide-halide displacement.

V. CONCLUSION

We have considered theoretically the solid phases of the hydrogen halides HF, HCl, and HBr under pressure, and

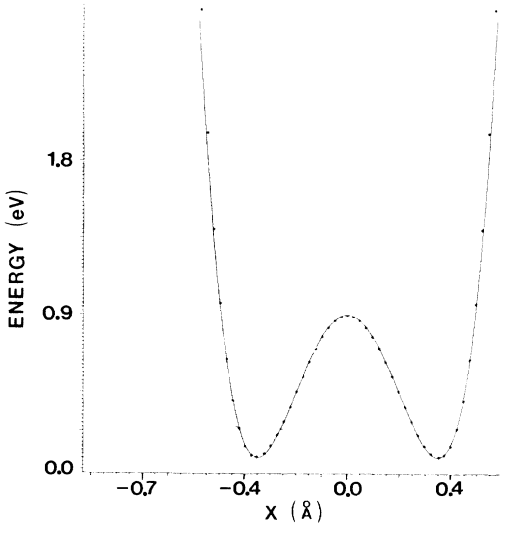

FIG. 18. Plot of the total energy for an H_6F_6 molecular ring as a function of the displacement (x) of the H atom from the midpoint between the F atoms along with the fit to the fourth power potential [Eq. (4)].

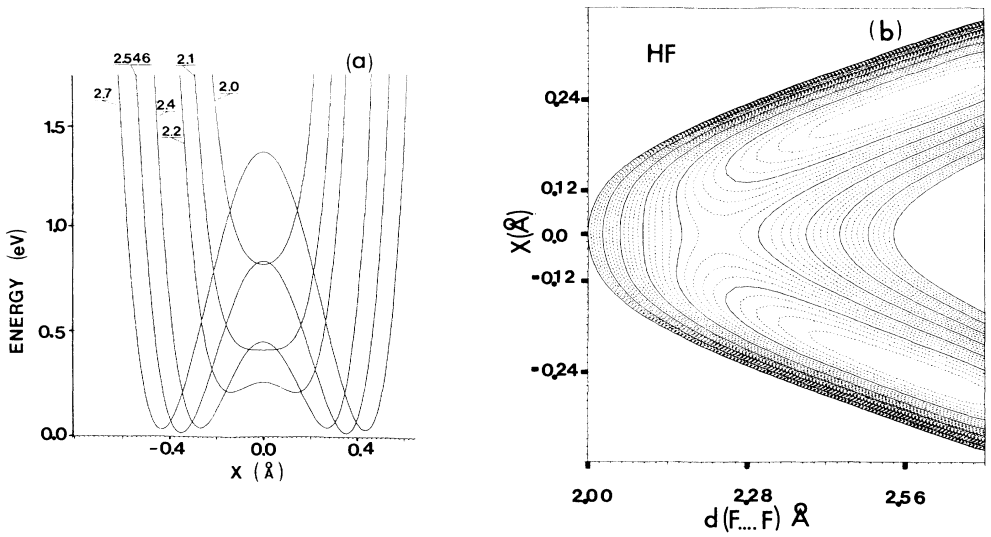

FIG. 19. (a) Total energy for H_6F_6 ring as a function of hydrogen position (x) for several choices of the F-F displacement d. (b) Contour plot of the total energy of an H_6F_6 ring relative to the global minimum as a function of the displacement (x) of the hydrogen from the midpoint position between the adjacent F atoms and the F-F displacement d (F · · · F).

have found them to be nearly model systems to study the transition from a hydrogen-bonded molecular crystal to a covalently bonded crystal. A simple model with very few parameters was used to describe the hydrogen-halide system, and, in particular, it was shown how pressure acts as a simple tuner for the nonlinearities of the system. The doubly degenerate ground state allows for the possibility of soliton formation, and the light mass of the hydrogen makes quantum effects important to consider for these materials. We find as pressure is increased, the barrier reduces rapidly, and the crystal undergoes a second-order phase transition from the asymmetric to the symmetric ground states. The inclusion of quantum effects did not drastically change the nature of the phase transition, but did change hydrogen symmetric stretch frequencies. *Ab initio* LDA calculations have been performed for HBr in a linear chain form and for an H_6F_6 molecular ring model for solid HF. These calculations lend support to many of the ideas of the simple model. It is found that at zero pressure the barrier between left and right ground states is large enough (0.8 eV and 0.6 eV for HF and HBr, respectively) so that very little hydrogen tunneling is expected to occur in the ground state. The hydrogen vibration frequencies derived from these models are in excellent agreement with experiment, as are the asymmetric displacements. At higher pressure we find the ground state goes to the symmetric bonded phase. This phase is found to occur when $d \simeq 3.25$ Å for HBr and at $d \simeq 2.15$ Å for HF where d is the halide-halide displacement.

ACKNOWLEDGMENTS

A grant from the Arizona State University Research Fund supported much of this work. One of us (A.I.K.) was supported in part by Associated Western Universities. Another (M.O'K.) was supported by a grant from the National Science Foundation. One of us (O.F.S.) also acknowledges partial support by the U. S. Office of Naval Research (under Contract No. ONR-N00014-85-K-0442).

*Also at Dipartimento di Scienze Fisiche dell'Università and Gruppo Nazionale di Struttura della Materia, Consiglio Nazionale delle Ricerche (GNSM-CNR), Cagliari, Italia.

[1]F. H. Stillinger and K. S. Schweizer, J. Phys. Chem. **87**, 4281 (1983); K. S. Schweizer and F. H. Stillinger, J. Chem. Phys. **80**, 1230 (1984).

[2]Y. R. Hirsch and W. B. Holzapfel, Phys. Lett. **101A**, 1230 (1984); J. Chem. Phys. **84**, 2771 (1986).

[3]A. Polium and M. Grimsditch, Phys. Rev. Lett. **52**, 1312 (1984).

[4]M. Atoji and W. N. Lipscomb, Acta Cryst. **7**, 173 (1954); R. B. Von Dreele, D. A. Pinnick, and R. C. Hanson, (unpublished).

[5]E. Sandor and R. F. C. Farrow, Nature **23**, 171 (1967); E. Sandor and M. W. Johnson, Nature **217**, 541 (1968); M. W. Johnson, E. Sandor, and E. Arzi, Acta Cryst. B **31**, 1998 (1975).

[6]S. P. Habuda and Y. V. Gagarinsky, Acta Cryst. B **27**, 1677 (1971).

[7]J. S. Kittelberger and D. F. Hornig, J. Chem. Phys. **46**, 3099 (1967).

[8]A. Anderson, B. H. Torrie, and W. S. Tse, Chem. Phys. Lett. **70**, 300 (1980).

[9]R. C. Hanson and A. Katz, *High Pressure Science and Technology,* Proceedings of the 9th AIRAPT Conference, Alang,

NY, 1983 (North-Holland, Amsterdam, 1984), p. 99; and (unpublished).
[10]P. G. Johannsen, W. Helle, and W. B. Holzapfel, J. (Paris) Colloq. **45**, C8-199 (1984).
[11]P. A. Giguere and N. Zengin, Can. J. Chem. **36**, 1013 (1958).
[12]M. L. N. Sastri and D. F. Hornig, J. Chem. Phys. **39**, 3497 (1963).
[13]S. A. Lee, D. A. Pinnick, S. M. Lindsay, and R. C. Hanson, Phys. Rev. B **34**, 2799 (1986).
[14]R. C. Hanson, A. I. Katz, and D. Pinnick (unpublished).
[15]J. van Straaten and I. F. Silvera, Phys. Rev. Lett. **57**, 766 (1986).
[16]A. Zunger, J. Chem. Phys. **63**, 1713 (1975).
[17]A. Karpfen, A. Beyer, and P. Schuster, Int. J. Quantum Chem. **19**, 1113 (1981).
[18]A. Beyer and A. Karpfen, Chem. Phys. **64**, 343 (1982).
[19]L. Pietronero and N. O. Lipari, J. Chem. Phys. **62**, 1976 (1975).
[20]T. E. Peacock and R. McWeeny, Proc. Phys Soc. **74**, 385 (1959).
[21]G. del Re, J. Ladik, and G. Biczo, Phys. Rev. **155**, 997 (1967).
[22]J. M. Andre, L. Gouverneur, and G. Leroy, Int. J. Quantum Chem. **1**, 451 (1967).
[23]J. Delhalle, L. Piela, J-L. Bredas, and J. M. Andre, Phys. Rev. B **22**, 6254 (1980).
[24]C. Kittel, in *Quantum Theory of Solids* (Wiley, New York, 1963), p. 25.
[25]R. D. Etters, V. Chandrasekharan, E. Uzan, and K. Kobashi, Phys. Rev. B **33**, 8615 (1986).
[26]For a review of solitons, see A. R. Bishop, J. R. Krumhansl, and S. E. Trullinger, Physica **1D**, 1 (1980), and references therein.
[27]A. S. Davydov, Phys. Scr. **20**, 387 (1979).
[28]H. Buttner and H. Bilz, J. Phys. (Paris) Colloq. **42**, C6-111 (1981).
[29]E. W. Laedke, K. H. Spatschek, M. Wilkins, Jr., and A. V. Zolotariuk, Phys. Rev. A **32**, 1161 (1985).
[30]St. Pnevmatikos, N. Flytzanis, and M. Remoissenet, Phys. Rev. B **33**, 2308 (1986).
[31]S. A. Brazovskii, L. P. Gorkov, and J. R. Schrieffer, Phys. Scr. **25**, 423 (1982).
[32]R. H. Baughman and G. Moss. J. Chem. Phys. **77**, 6321 (1982).
[33]P. Hohenberg and W. Kohn, Phys. Rev. **136**, B864 (1964).
[34]W. Kohn and L. J. Sham, Phys. Rev. **140**, A1133 (1965).
[35]M. Gell-Mann and K. Bruechner, Phys. Rev. **106**, 364 (1957).
[36]D. M. Ceperly, Phys. Rev. B **18**, 3126 (1978).
[37]D. M. Ceperly and B. J. Alder, Phys. Rev. B **45**, 566 (1980).
[38]J. P. Perdew and A. Zunger, Phys. Rev. B **23**, 5048 (1980).
[39]O. Gunnarson, B. I. Lundqvist, and J. M. Wilkins, Phys. Rev. B **10**, 1319 (1974).
[40]H. B. Shore, J. H. Rose, and E. Zaremba, Phys. Rev. B **15**, 2858 (1977).
[41]K. Schwarz, Chem. Phys. Lett. **57**, 605 (1978).
[42]D. R. Hamann, M. Schluter, and C. Chiang, Phys. Rev. Lett. **43**, 1494 (1979).
[43]G. B. Bachelet, D. R. Hamann, and Schluter, Phys. Rev. B **26**, 4199 (1979).
[44]J. Ihm, A. Zunger, and M. L. Cohen, J. Phys. C **12**, 4409 (1979).
[45]S.-Y. Liu, D. W. Michael, C. E. Dykstra, and J. M. Lisy, J. Chem. Phys. **84**, 5032 (1986).
[46]T. Emsley, R. J. Parkev, and R. E. Overill, J. Chem. Soc. Faraday Trans. **2**, 1347 (1983).
[47]M. O'Keefee, J. Amer. Chem. Soc. **108**, 4241 (1986).
[48]H. Lischka, Chem. Phys. Lett. **66**, 108 (1979).
[49]P. C. Hariharan and J. A. Pople, Theor. Chim. Acta. **28**, 213 (1973).
[50]A. Anderson, B. H, Tornie, and W. S. Tse, J. Raman Spectrosc. **10**, 148 (1981).
[51]R. L. Redingtion, J. Phys. Chem. **86**, 552 (1982).